Available online at www.sciencedirect.com

ScienceDirect

Procedia Computer Science 126 (2018) 472–481

Procedia Computer Science

www.elsevier.com/locate/procedia

International Conference on Knowledge Based and Intelligent Information and Engineering Systems, KES2018, 3-5 September 2018, Belgrade, Serbia

Automatic Segmentation of Diffuse Retinal Thickening Edemas Using Optical Coherence Tomography Images

Gabriela Samagaio[a,b], Joaquim de Moura[a,b,*], Jorge Novo[a,b], Marcos Ortega[a,b]

[a] *Department of Computing, University of A Coruña, A Coruña, Spain*
[b] *CITIC - Research Center of Information and Communication Technologies, University of A Coruña, A Coruña, Spain*

Abstract

Diabetic retinopathy is one of the leading causes of vision impairment that is commonly associated to the Macular Edema (ME) disease. The Diffuse Retinal Thickening (DRT) is a ME type derived from the local intraretinal fluid accumulation in the lower retinal layers, producing significant morphological alterations in the eye fundus. The presence and properties of these intraretinal fluids are used by the ophthalmologists as significant indicators of the clinical stage of the ME disease. Given that, the precise identification and segmentation of the DRT edema type allow the early diagnosis of the ME disease which, therefore, permits a better adjustment of the treatments, reducing their costs as well as improving the life quality of the patients.

This paper proposes a novel methodology for the automatic identification and segmentation of the DRT edemas using Optical Coherence Tomography (OCT) images as source of information. Firstly, the method identifies four of the principal retinal layers that are used as reference to delimit the outer retina, region where the DRT edemas are typically originated. Inside this region, a large and heterogeneous set of features was defined to recognize the characteristic "sponge-like" patterns of the DRT edema, using intensity, texture and clinically-defined features. For this analysis, four representative classifiers were employed with the best subsets of previously selected features. This methodology was tested using 70 OCT images from where 560 samples were extracted with the presence and absence of DRT edemas. The best results were achieved by the 7-*k*NN classifier, reaching in the detection stage an accuracy of 0.9366, whereas in the segmentation stage obtained values of 0.6625 and 0.7899 for the Jaccard and Dice coefficients, respectively.

Keywords: Computer-aided diagnosis; optical coherence tomography; diffuse retinal thickening region; segmentation

1. Introduction

Macular Edema (ME) is characterized as a nonspecific retinal eye disease with painless visual acuity impairment. It is caused by a leak of fluid derived from the blood of the vascularity within the retinal tissue[1]. The presence of this fluid accumulation within the retina leads to significant modifications of the morphology of this tissue (especially regarding its thickness), producing the main alterations to the lower retinal layers[2]. Given that the retina constitutes

* Corresponding author. Tel.: +34-881011330; fax: +34-981167160.
E-mail address: joaquim.demoura@udc.es

10.1016/j.procs.2018.07.281

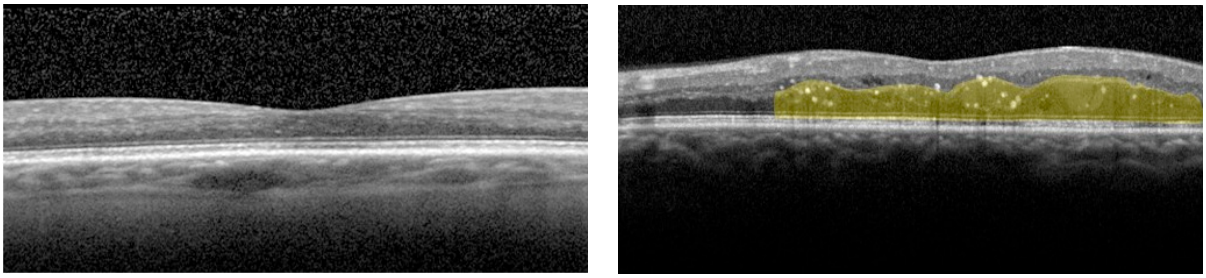

(a) (b)

Fig. 1. Example of OCT images. (a) Healthy retinal tissue. (b) Retina with the DRT edema presence (yellow).

the light-sensitive tissue at the back of the eye, and the macula is the part of the retina that is responsible for the sharp, central and color vision, this fluid accumulation leads to the deterioration of the vision quality and, in more advanced clinical stages, it could lead to complete blindness. According to the World Health Organization (WHO), the major global causes of moderate to severe vision impairment are Age-related Macular Degeneration (AMD) and Diabetic Retinopathy (DR), affecting a 4% and 1%, respectively, of the world population[3]. In fact, these diseases have as common denominator for the visual loss perception the ME formation within the retinal tissue[4]. In particular, one of the most spread diseases over the world is diabetes, in which the lack of insulin causes a higher presence of glucose in the circulatory system[5]. These unhealthy concentrations damage the blood vessels, consequently deteriorating the retinal microcirculation and producing these fluid accumulations (or edemas), what is clinically defined as Diabetic Macular Edema (DME)[6,7].

To identify the presence of these pathological structures in the retinal tissue, Optical Coherence Tomography (OCT) imaging is being widely used within the ophthalmological community[8]. Its great acceptance is given by the favorable characteristics of this image modality for this analysis, offering an easy visualization of the in vivo histopathology of the retinal tissue in a contactless and non-invasive capture process. Given that, it is widely recognized as a comfortable medical examination for both patients and clinicians, showing with detail the inner characteristics of the retinal layers. This medical image modality offers exhaustive information of the retinal tissue, facilitating the diagnosis of the ME presence by the identification of significant modifications in the morphology of the retinal layers which are commonly caused by the intraretinal fluid accumulation[9].

According to Otani *et al.*[10], OCT images offer important clinical information that enables the identification and classification of the ME disease in three different types: Serous Retinal Detachment (SRD), Cystoid Macular Edema (CME) and Diffuse Retinal Thickening (DRT). Following the same classification, Panozzo *et al.*[11] established five criterions to better identify and individually characterize each type of ME, being the following: retinal thickness, diffusion, volume, morphology and presence of the vitreous traction[12]. These criterions are based on the unique pathophysiology that each type of ME adopts within the retinal tissue, mainly delimited between the Inner Limiting Membrane (ILM) and the Retinal Pigment Epithelium (RPE), superior and inferior boundaries, respectively.

Regarding the DRT edemas, they are typically recognized by the specialists as a retinal swelling of the macula with reduced intraretinal reflectivity. Figure 1 presents a couple of examples of normal and pathological retinal cases with the DRT edema presence and absence. The absence of a limiting membrane in this ME type allows the fluid spread over the retina, resulting in a "sponge-like" swelling appearance. As result, the thickness of the lower retina region increases, which consequently leads to an increment of the entire retinal thickness, modifying significantly the normal morphology and patterns of the eye fundus tissue[13]. Moreover, given that this ME type typically appears before CME and SRD edemas, it is commonly used by ophthalmologists as a relevant biomarker for the early diagnosis of the ME disease. Based on those premises, a precise detection and segmentation of the DRT edemas is crucial, given it facilitates the early diagnosis of the disease, allowing a better adjustment of the treatments which consequently reduces costs and improves the life quality of the patients.

Given this relevance, in the recent years, some works were published using OCT images for the identification and characterization of the ME disease. As reference, Sun *et al.*[14] proposed an automatic approach to detect and segment the SRD edemas. Firstly, the authors delimit the abnormal retinal layers by the application of a multi-scale

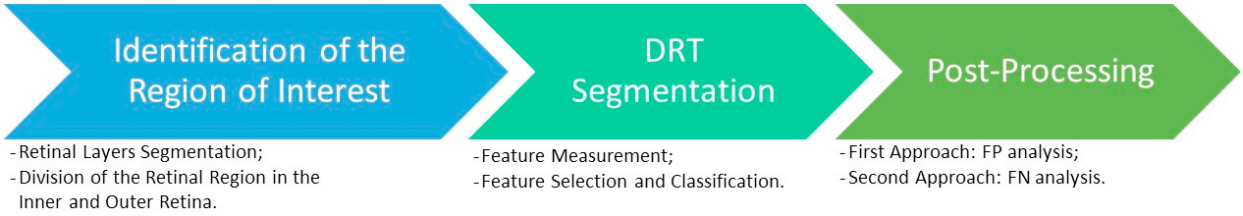

Fig. 2. Main stages of the proposed methodology for the DRT region identification and segmentation.

graph search method. Then, using AdaBoost, the ME region is segmented using a total of 62 features. In the work proposed by Moura *et al.* [15], the proposed methodology was designed to automatically identify the intraretinal cystoid fluid regions in OCT images. As a first stage, the authors used a window of a given size to determine the presence of hypothetical candidates of cystoid regions. Then, learning approaches were applied to extract a set of image characteristics that determine the presence of cysts inside the analyzed regions. In the work of Schleg *et al.* [16], a deep learning approach was implemented by performing a neural network comprising two processing components to classify regions in the retina as normal tissue or macular fluid regions as SRD or CME. Following a similar strategy, Rashno *et al.* [17] proposed a method using a neutrosophic transformation and a graph-based shortest path to segment fluid-associated and cystoid regions. Gopinath *et al.* [18] proposed a methodology using a Convolutional Neural Network (CNN) as a deep learning strategy for the segmentation of CMEs followed by a post-processing step using a clustering method to refine the previously identified cystoid regions. Regarding the DRT edemas, Samagaio et al. [19] addressed the automatic detection of the three types of ME in the OCT images. Despite that in the last few years some studies addressed the automatic identification and segmentation of the intraretinal fluid, mainly for the cystoid case, in OCT images, to date, no other scientific proposal studied the issue with the DRT edema type.

In this way, we propose in this work a new methodology that faced the automatic identification and segmentation of the DRT presence in OCT images using as reference the clinical classification in the ophthalmological field [10,11]. Firstly, the region where these edemas typically emerge is identified, the outer retina. Then, a learning strategy was implemented that analyzes windows of a defined size, extracting a complete and heterogeneous set of intensity, texture and clinically-defined image characteristics to precisely identify and segment the presence of the DRT edema type. Finally, a post-processing stage was implemented to refine the results and improve the efficiency of the proposed method.

2. Methodology

The proposed methodology is composed by a set of progressive stages for the identification and segmentation of DRT edemas, as represented in Fig. 2. Firstly, the system segments the retinal layers to facilitate the search of this ME type in the Region of Interest (ROI) where they typically appear, the outer retina. Then, a learning strategy is applied to identify the DRT presence and segment its constituent region. Finally, a post-processing strategy is implemented to individually refine the impact of the FP and the FN detected regions from the classifier output and improve the obtained results. In the following subsections these steps are described in detail.

2.1. Identification of the Region of Interest

This stage of the methodology is sub-divided in two main steps: the retinal layer segmentation and its division in the inner and outer retina, being the latter where the DRT edemas are spread.

2.1.1. Retinal Layer Segmentation

DRT edemas are recognized by the specialists as a drop of the intensities in the outer retina with an undefined morphological shape and a “sponge-like” appearance. The absence of an enclosing membrane allows the fluid spread over the lower retinal tissues, the outer retina. As a result of the intraretinal fluid accumulation, the outer retina suffers a significant thickness increment, which leads consequently to an increase of the entire ROI thickness.

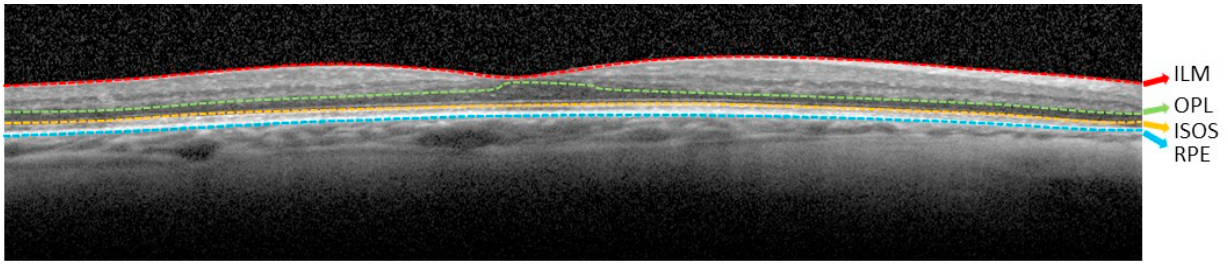

Fig. 3. Example of OCT image with the identification of the aimed four retinal layers: ILM, OPL, ISOS and RPE.

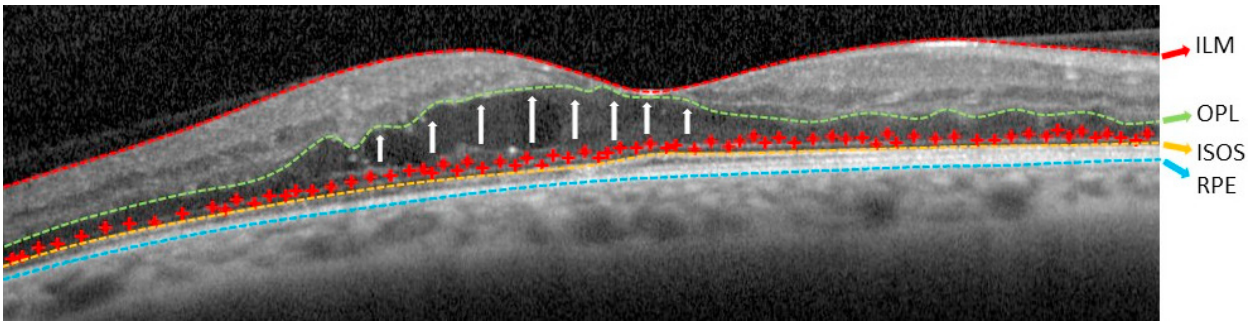

Fig. 4. Example of OCT image with a schematic representation of the OPL layer identification. The arrows (↑) indicate the direction of the applied region growing algorithm using N seeds (+) over the ISOS layer.

Therefore, the proposed system firstly identifies four retinal layers: the ILM, the Outer Plexiform Layer (OPL), the Inner Segment/Outer Segments (ISOS) of the photoreceptors layer and the RPE, as illustrated in Fig. 3. These layers serve to delimit the inner and outer retina which permits, therefore, the restriction of the search space to identify the DRT presence. To achieve the identification of the ILM, ISOS and the RPE retinal layers, we implemented an approach based on the work of Chiu *et al.*[20]. This approach mainly uses graph theory and dynamic programming, using the OCT images as a graph of nodes. This strategy connects pixels, forming pathways from both sides of the image from where the optimal paths provide the aimed layers. The algorithm calculates dark-to-light gradient images, identifying adjacent layers and generating weights for the layer segmentation. The main layers of the retina are identified progressively by the minimum weighted paths using the Dijkstra algorithm[21]. This way, we extract the ILM, ISOS and RPE retinal layers.

Regarding the OPL layer, we designed a different specific strategy given that the DRT presence leads to a significant change in the retinal tissue, implying consequently a deterioration of the conditions of this retinal layer, hardening enormously its extraction. Thus, to solve this issue, the previously identified ISOS layer is used as baseline. Over it, N initial points are randomly generated and used as seeds with a region growing approach[22], process that is illustrated in Fig. 4. Using as reference the image dimensions, the number of generated seeds is a proportional 10% of the input image width. This approach enables the pixel aggregation by appending the seed neighborhood of pixels with similar intensity properties. Therefore, we obtain the entire region over the ISOS layer by intensity similarity. From the resultant region, the identification of the OPL layer is provided by the upper limit of the extracted region.

2.1.2. Division of the Retinal Region in the Inner and Outer Retina

Its relative position is one of the main characteristics that is used by the specialists to recognize the DRT presence in the retina. As said, typically, DRT edemas appear in the outer retinal layers, defined as the lower region of the retina. Therefore, to facilitate the search process, the previously identified retinal ROI is subdivided in two sub-regions: the inner and the outer retina, as represented in Fig. 5. The inner retina defines the upper region of the ROI which is comprehended between the ILM and the OPL layers as the superior and inferior limits, respectively. The outer

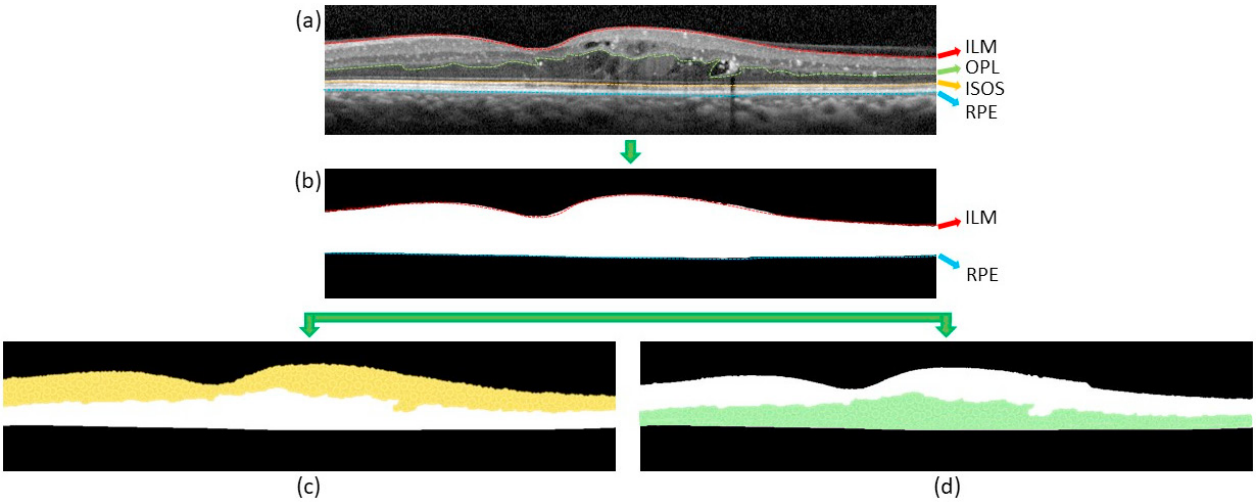

Fig. 5. Identification of the inner and outer retinal regions. (a) Example of OCT image. (b) Identification of the retinal region limited by the ILM and RPE layers. (c) The inner retina, between the ILM and OPL layers. (d) The outer retina, between the OPL and ILM layers.

retina is the lower region delimited by the OPL and RPE layers. Therefore, using the previous layer extractions, the system searches for the DRT presence in the OPL/RPE region, removing the ILM/ISOS region. We also exclude the ISOS/RPE region to further reduce the search space, given also the absence of DRT edemas at that level of the eye fundus.

2.2. DRT Segmentation

Using the previously identified outer retina, next, we perform the identification and segmentation of the DRT edemas in the restricted search space. Given that, we designed a methodology that exploits the image information of this region with a machine learning strategy, herein described with more detail.

2.2.1. Feature Measurement

In order to characterize each analyzed region as with DRT and non-DRT presence, a total of 307 features were extracted from the analyzed regions of the outer retina. Given that these edemas neither present well-defined boundaries nor a characteristic morphological shape, a suitable combination of features were analyzed that are based on intensity, texture and domain information. More specifically, these edemas are recognized by their typical tissue patterns as well as the consequent thickness increment of the retinal region. These features are extracted from a window of a variable height, corresponding to the maximum column height of the region of the outer retina under analysis. The analyzed features are summarized in Table 1.

2.2.2. Feature Selection and Classification

Given the high dimensionality of the set of features, we applied a feature selector to avoid irrelevant and redundant characteristics. In particular, the Sequence Forward Selection (SFS)[23] was employed to determine the feature subset that better predicts the DRT presence, facilitating the classification stage. This selector adds features to the subset by an incremental importance feature order. Then, using the final subset of features, four representative classifiers were trained and tested, such as: the Naive Bayes, the k-Nearest Neighbors (kNN), the Parzen and the Quadratic Bayes Normal Classifier (QDC). In the case of the kNN, 3 configurations were tested, using values of k = [3, 5, 7]. To measure the capacity of the classifiers, the dataset was randomly divided in two smaller sets with the same size (each one with the 50% of all the samples), being processed with a 10-fold cross-validation. The first dataset is used for the training stage whereas the second one is reserved for testing the trained classifiers. This process of dataset random division, training and testing was repeated 50 times, calculating the final mean accuracy as result for the

Table 1. List of the defined set of 307 features to identify the DRT presence.

Category	Features
Global Intensity-Based Features (GIBS)	[1-15] Maximum, minimum, mean, median, std, variance, 25^{th} percentile, 75^{th} percentile, skewness and maximum likelihood estimates for normal distribution.
Gray - Level Co-Ocurrence Matrix (GLCM)	[16-31] Contrast, energy, correlation and homogeneity.
Histogram of Oriented Gradients (HOG)	[32-112] 9 windows per bound box and 9 histogram bins.
Gabor	[113-240] Mean and std. Orientations = 8 and scale =8.
Local Binary Pattern (LBP)	[241-304] Mean and std. Number of neighbors = (4, 8, 12, 16) and filter radius: 1-8.
Retinal Thickness Analysis	[305-307] Thickness analysis: OPL/ISOS, ILM/RPE and the ratio between the OPL/ISOS and ILM/ISOS regions.

global performance measurement. As output of this stage, the columns within the outer retina are classified with DRT or non-DRT presence, being the region of the outer retina of the column extracted for the DRT segmentation.

2.3. Post-Processing

Finally, we implemented a post-processing stage in the outer retinal region using as reference the results from the classifier that achieved the best performance for the DRT detection. In order to improve the performance of the proposed method for the segmentation of the DRT region, two independent approaches were designed and analyzed. The first approach aims the FPs removal, false detections that are introduced by other retinal structures, whereas the second approach tests the aggregation of non-consecutive DRT regions, with the aim of reducing the rates of FNs.

Firstly, the presence of artifacts and/or pathological and retinal structures as hard exudates or vessels generates shadows in the retinal layers that may enormously alter the analysis. As shown in Fig. 6(a), these shadows typically create dark patterns that may be confused with the drop of intensities of the DRT presence, leading to the erroneous identification and segmentation of these regions as DRT edemas (FPs)[24]. In this way, we implemented a strategy to analyze the influence of the FP rates, using two designed parameters: minimum width of each set of DRT columns and the distance to the subsequent closer DRT region.

Secondly, as illustrated in Fig. 6(b), the presence of CMEs with relatively large dimensions in the outer retina frequently creates miss-classified regions. These regions are wrongly classified as non-DRT regions, given that the presence of, for example, hyperreflective membranes of the CMEs create bright patterns with different properties than the typical DRT regions in the outer retina. Moreover, the presence of bright artifacts in the outer retina could be also confused with non-DRT edemas, increasing the FN rates. Given that, we implemented a post-processing approach to analyze the influence of these misclassified regions. To this aim, we implemented an aggregation factor that connects two consecutive detected DRT regions, if the distance between them is smaller than the defined value of the aggregation factor. Given that, we assume that both non-consecutive regions belong to the same DRT edema, by unifying the unconnected detections of the classifier.

Using both strategies, we measured their impact in the global performance of the proposed system for the DRT segmentation and the corresponding increment of the obtained efficiency.

3. Results and Discussion

The proposed method was validated using a dataset that is composed by 70 OCT images. This dataset was acquired with a Spectralis® OCT confocal scanning laser ophthalmoscope from Heidelberg Engineering. The scans are centered in the macula with a resolution that varies from 401×1015 to 481×1521 pixels. The images correspond to scans from both left and right eyes of different patients that were diagnosed with ME.

In order to test the performance of the proposed work, the images were labeled by an expert clinician, identifying the regions that presented DRT edemas. Using this information, we constructed a dataset by the extraction of the 307 defined features for 560 samples with non-DRT and DRT edema presence. The constructed dataset was randomly divided in two subsets with the same size, one for training and other for testing, without the application of any

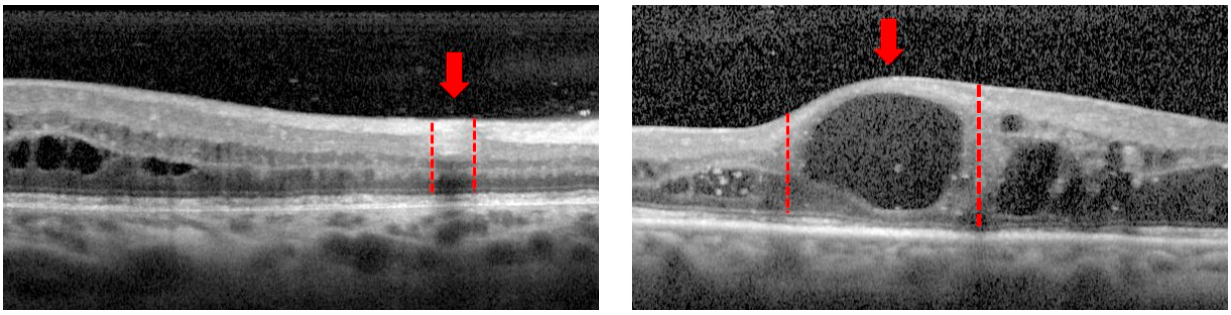

(a) (b)

Fig. 6. Example of OCT images. (a) Presence of shadows generates FP detections. (b) Presence of CME with a relative large dimensions and hyperreflective membrane generates FN detections.

preprocessing to the input images. Then, the features were obtained with the same defined window size in the test and validation stages of the methodology. As said, to ensure the accuracy of the global performance, we trained the model using a 10-fold cross-validation with a total of 50 repetitions, being calculated the mean error/accuracy to measure the final performance of the method.

In particular, we analyzed the efficiency of the proposed system in three main stages: firstly, we tested the detection of DRT columns; then, we validated the segmentation results; and finally, we analyzed the post-processing strategies to determine their influence in the reduction of the FPs and FNs rates, using the best trained classifier.

To detect the DRT edemas within the outer retina, we firstly determined the subset of features that better discriminate the presence of this ME type by the application of the SFS strategy until there is no improvement in the identification process. The majority of the selected features were taken from Gabor, LBP and HOG categories, as they present a high capacity of differentiation between healthy retinal layer patterns and pathological regions as DRT edemas. The thickness of the ILM/RPE and the ratio between the OPL/ISOS and ILM/RPE regions also presented a significant relevance, being selected in the first positions given that DRT edemas imply not only an increment of the outer retina thickness but also the increment of the entire "retinal thickening".

Table 2 details the results that were achieved by the method using different classifiers and configurations, as well as the application of progressive larger feature sets. A maximum of 55 selected features were established as no further improvements were obtained from that size.

Table 2. Accuracy results that were obtained with the tested classifiers using different feature sets sizes.

N. Features	5	15	25	35	45	55
Naive Bayes	0.8898	0.9024	0.8889	0.8764	0.8716	0.8696
3-*k*NN	0.9086	0.9202	0.9236	0.9269	0.9293	0.9252
5-*k*NN	0.9068	0.9253	0.9274	0.9283	0.9282	0.9241
7-*k*NN	0.9100	0.9298	0.9252	0.9265	0.9275	0.9210
Parzen	0.9082	0.9245	0.9299	0.9278	0.9299	0.9281
QDC	0.9044	0.9202	0.9302	0.9257	0.9223	0.9163

Also, Table 3 presents the best feature set sizes for each classifier configuration and the corresponding obtained accuracy. Generally, the obtained results in all the cases are satisfactory, being above a 0.86 of accuracy even for relatively small subsets of selected features. From all of them, the best result was achieved with the 7-kNN and 21 selected features, returning a performance of 0.9366. On the contrary, the worst results were obtained using the Naive Bayes classifier with a value of 0.9074 of accuracy and 20 selected features, also representing a satisfactory result. With respect to the Parzen and QDC classifiers, both also offered an adequate performance, reaching accuracy values of 0.9351 and 0.9335 with 43 and 30 selected features, respectively, at a close distance of the 7-kNN classifier performance, reinforcing the validity of the designed methodology.

Table 3. Accuracy results that were obtained with the tested classifiers using different features set sizes.

Classifier	Naive Bayes	3-*k*NN	5-*k*NN	7-*k*NN	Parzen	QDC
N. Features	20	46	18	21	43	30
Accuracy	0.9074	0.9310	0.9346	0.9366	0.9351	0.9335

We also tested the influence of the dimensions of the window size in the training and testing stages of the methodology. Each window is centered in the column under analysis using progressively larger window sizes and variable heights (h), as previously described. Table 4 details the best performance that was achieved for each window size combined with the best configuration of the analyzed classifiers. As we can see, the best accuracy result was obtained with a $h \times 23$ window size. Smaller window sizes do not offer the same satisfactory results, given that it does not contain sufficient significant information to distinguish the DRT texture from the surrounding healthy tissue. On the other hand, using too large window sizes, as $h \times 33$, the extracted features do not incorporate new information from the DRT regions, being the obtained accuracy relatively similar to the best window size.

Table 4. Best accuracy obtained by each tested classifier using different window sizes.

Window size	$h \times 5$	$h \times 11$	$h \times 17$	$h \times 19$	$h \times 23$	$h \times 25$	$h \times 29$	$h \times 33$
7-*k*NN	0.8866	0.9076	0.9170	0.9210	0.9366	0.9197	0.9331	0.9291

The segmentation stage of the methodology is based on the previous DRT detection, using as reference the height of the outer retina. To validate the performance of this stage, we used as reference two statistical metrics that are commonly used in the literature for similar purposes: Jaccard and Dice coefficients. Moreover, to further improve the efficiency of the segmentation stage, we analyzed the performance of the mentioned post-processing approaches for the FP and FN rates reduction. Table 5 presents a comparative analysis using accuracy, Jaccard and Dice coefficients for the three tested approaches: no post-processing, using the first post-processing strategy and using the second post-processing strategy. As we can see, the results from the classifier without any post-processing strategy are satisfactory, achieving a 0.6106 and 0.7480 of Jaccard and Dice coefficients, respectively. Figure 7 shows an example of resultant OCT image after the application of the first post-processing approach. As we can see, the presence of artifacts in the outer retina produces wrong detections. Given that, the first post-processing approach analyzes the best combination of the optimal FP width (w_{min}) and the distance to the closer DRT columns (d_{min}), in order to reduce the FPs from the classifier output. Hence, the best accuracy was obtained using values of w_{min} and d_{min} of 16 and 10, respectively, resulting in an increase of 1% of the Jaccard and the Dice coefficients. Therefore, we can conclude that this strategy offers a slight improvement on the segmentation performance of the DRT regions.

Table 5. Accuracy , Jaccard and Dice coefficients for the segmentation stage using the best configuration classifier.

Classifier	No Post-Processing			First Post-Processing					Second Post-Processing			
	Accuracy	Jaccard	Dice	w_{min}	d_{min}	Accuracy	Jaccard	Dice	d_{af}	Accuracy	Jaccard	Dice
7-*k*NN	0.8381	0.6106	0.7480	16	10	0.8437	0.6162	0.7516	34	0.8668	0.6625	0.7899

The second post-processing approach tests the influence of the FN classified regions in the precise performance of the DRT region segmentation. From the implementation of this approach, the Jaccard and Dice coefficients achieved satisfactory results reaching values of 0.6625 and 0.7899, respectively. Comparing these coefficients with the results from the output of the classifier, it is possible to verify the significant improvement of 5% and 4% for Jaccard and Dice coefficients, respectively. Figure 8 presents an illustrative result image from the implementation of this second post-processing approach, where we can verify that the unification of non-consecutive DRT regions improves the efficiency of the method.

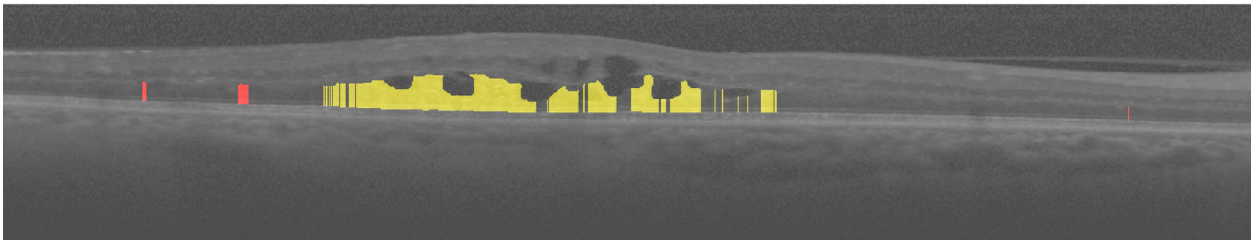

Fig. 7. Illustrative output OCT image after the application of the first post-processing approach. Yellow regions, direct result of the classifier. Red regions, removed columns by the application of the first post-processing approach.

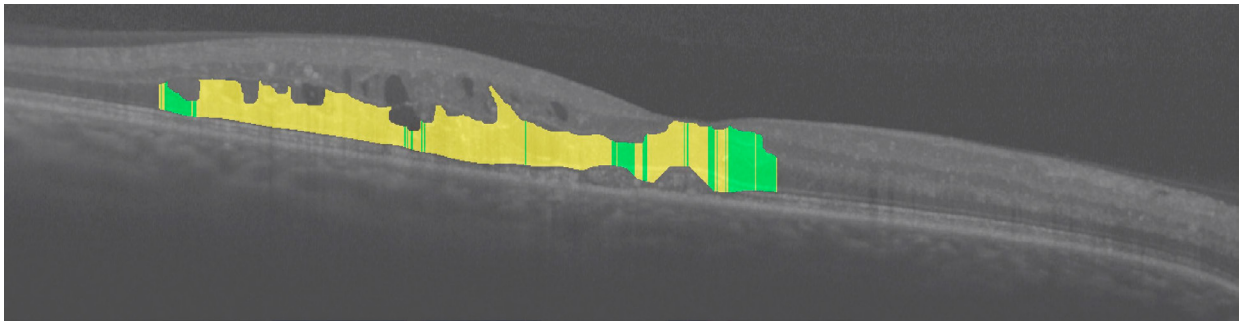

Fig. 8. Illustrative output OCT image after the application of the second post-processing approach. Yellow regions, direct results from the classifier. Green regions, result of the second post-processing approach.

Summarizing, despite the accurate performance of the different configurations, we can conclude that the best configuration for the segmentation of the DRT edema regions includes the use of the 7-*k*NN classifier followed, especially, by the application of the second post-processing approach.

4. Conclusions

The precise identification and quantification of the DRT edemas are crucial tasks for the early diagnosis of a relevant disease as is the Macular Edema, among the main causes of blindness in the developed countries. Additionally, a precise segmentation of the entire DRT region represents a tedious and hard issue given the absence of limiting membranes as well as the lack of contrast of its constituting region.

Given that, in this work, a new methodology for the automatic identification and segmentation of DRT edemas using OCT images is proposed. As said, to date, no other work faced the identification and segmentation of the DRT type of the relevant disease as is the Macular Edema. Firstly, we restricted the search space of these edemas using, as reference, four principal retinal layers that are initially segmented: ILM, OPL, ISOS and RPE layers. These layers permit the restriction of the search space to the outer retina, region where the DRT edemas are originated. In this restricted region, a complete and heterogeneous set of 307 features were extracted within windows of a defined size. Given the high dimensionality of the feature set, the SFS feature selector was applied, reducing the dimensionality of the feature set as well as providing to the classifier the most useful subset of features. Representative classifiers were trained to discriminate the DRT presence. Using the best classifier configurations, we applied post-processing strategies that address two different ways of facing the FP and FN influence in the performance of the proposed method, improving the obtained results. Satisfactory results were obtained, being the best performance achieved by the 7-*k*NN classifier using 21 features, providing a 0.6625 and a 0.7899 of Jaccard and Dice coefficients, respectively. As future works, a further analysis should be done to include more suitable characteristics as well as test different features selectors as wrapped-based methods. In addition, the performance of others classifiers should be analyzed, as neural networks.

Acknowledgements

This work is supported by the Instituto de Salud Carlos III, Government of Spain and FEDER funds of the European Union through the PI14/02161 and the DTS15/00153 research projects and by the Ministerio de Economía y Competitividad, Government of Spain through the DPI2015-69948-R research project. Also, this work has received financial support from the European Union (European Regional Development Fund - ERDF) and the Xunta de Galicia, Centro singular de investigación de Galicia accreditation 2016-2019, Ref. ED431G/01; and Grupos de Referencia Competitiva, Ref. ED431C 2016-047.

References

1. Marmor M. Mechanisms of fluid accumulation in retinal edema. *Macular Edema* 2000; p. 35-45.
2. Tranos P, Wickremasinghe S, Stangos N, Topouzis F, Tsinopoulos I, Pavesio C. Macular edema. *Survey of ophthalmology* 2004; **49**:470-490.
3. World Health Organization. World health statistics 2010. 2010; *World Health Organization*.
4. Schaal S, Henry J. Cystoid macular edema: medical and surgical management. *Springer* 2016.
5. Varma R, Bressler N, Doan Q, Gleeson M, Danese M, Bower J et *al.*. Prevalence of and risk factors for diabetic macular edema in the United States. *JAMA ophthalmology* 2015; **132**:1334-1340.
6. Fong D, Aiello L, Gardner T, King G, Blankenship G, Cavallerano J et *al.*. Retinopathy in diabetes. *Diabetes care* 2004; **1**:S84-87.
7. Miller K, Fortun J. Diabetic macular edema: current understanding, pharmacologic treatment options, and developing therapies. *Asia-Pacific journal of ophthalmology* 2018; **7**:28-35.
8. Gupta V, Gupta A, and Dogra M. Atlas of optical coherence tomography of macular diseases. *CRC Press* 2004.
9. Seo K, Yu S, Kim M, Kwak H. Visual and morphologic outcomes of intravitreal ranibizumab for diabetic macular edema based on optical coherence tomography patterns. *Retina* 2016; **36**:588-595.
10. Otani T, Kishi S, Maruyama Y. Patterns of diabetic macular edema with Optical Coherence Tomography. *American journal of ophthalmology* 1999; **127**:688-693.
11. Panozzo G, Parolini B, Gusson E, Mercanti A, Pinackatt S, Bertoldo G, Pignatto S. Diabetic macular edema: an OCT-based classification. *Seminars in ophthalmology* 2004; **19**:13-20.
12. Baamonde S, de Moura J, Novo J, Ortega M. Automatic detection of epiretinal membrane in OCT images by means of local luminosity patterns. *In international work-conference on artificial neural networks* 2017; p. 222-235.
13. Kim B, Scott D, Peter K. Optical coherence tomographic patterns of diabetic macular edema. *American journal of ophthalmology* 2006; **142**: 405-412.
14. Shi F, Chen X, Zhao H, Zhu W, Xiang D and et *al.*. Automated 3-D retinal layer segmentation of macular optical coherence tomography images with serous pigment epithelial detachments. *IEEE transactions on medical imaging* 2016 **34**:441-452.
15. Moura J, Novo J, Rouco J, Penedo M, Ortega M. Automatic identification of intraretinal cystoid regions in Optical Coherence Tomography. *Springer* 2017; p.305-315.
16. Schlegl T, Waldstein SM, Bogunovic H, Endstraßer F, Sadeghipour A, Philip AM, Podkowinski D, Gerendas BS, Langs G, Schmidt-Erfurth U. Fully automated detection and quantification of macular fluid in OCT using deep learning. 2017 *Ophthalmology*.
17. Rashno A, Koozekanani D, Drayna P, Nazari B, Sadri S, Rabbani H, Parhi K. Fully automated segmentation of fluid/cyst regions in Optical Coherence Tomography images with diabetic macular edema using neutrosophic sets and graph algorithms. *IEEE Transactions on Biomedical Engineering* 2017; **65**:989-1001.
18. Gopinath K, Sivaswamy J. Segmentation of retinal cysts from Optical Coherence Tomography volumes via selective enhancement. *IEEE Journal of Biomedical and Health Informatics* 2018.
19. Samagaio G, Estévez A, de Moura J, Novo J, Fernández M, Ortega M. Automatic identification of macular edema in optical coherence tomography images. *VISIGRAPP'18. 14th International joint conference on computer vision, imaging and computer graphics theory and applications* 2018; **4**:533-540.
20. Chiu S, Li X, Nicholas P, Toth C, Izatt J, Farsiu S. Automatic segmentation of seven retinal layers in SDOCT images congruent with expert manual segmentation. *Optics express* 2010; **18**:19413-19428.
21. Dijkstra E. A note on two problems in connexion with graphs. *Numerische mathematik* 1959; **1**:269-271.
22. Zhu S, and Alan Y. Region competition: unifying snakes, region growing, and bayes/MDL for multiband image segmentation. *IEEE transactions on pattern analysis and machine intelligence* 1996; **18**:884-900.
23. Efroymson M. Multiple regression analysis. *Mathematical methods for digital computers* 1960.
24. de Moura J, Novo J, Charlón P, Barreira N, Ortega M. Enhanced visualization of the retinal vasculature using depth information in OCT. *Medical & biological engineering & computing* 2017; **55**:2209-2225.